Effect of cap rock thickness and permeability on geological storage of CO_2: laboratory test and numerical simulation

Zhixi Chen, Fengde Zhou* and Sheikh S. Rahman
School of Petroleum Engineering, University of New South Wales, Sydney, NSW 2052, Australia
**Author for corresponding. E-mail: zhoufengde@gmail.com*

(Received 19 August 2013; accepted 16 November 2014)

Abstract

Geological storage of CO_2 is considered widely as an efficient method of mitigation of greenhouse gas emission. CO_2 storage mechanism includes structural trapping, residual gas trapping, solubility trapping and mineral trapping. The shale cap rock acts as a seal for the storage when CO_2 accumulates at the top of the reservoir. The injected CO_2 may migrate through the cap rock under buoyancy force or pressure build-up which depends on the seal capacity of the cap rock. As a result, the effectiveness of containment of injected CO_2 in the reservoir is largely dependent on the migration rate of CO_2 through the cap rock. This paper investigates the effects of CO_2 leakage through cap rock by a combination of experimental studies and numerical simulation. Firstly, experimental measurements on shale core samples collected from Australian cap rocks were conducted to determine properties, such as capillary pressure, pore size distribution and permeability. Based on the measured cap rock properties, the effect of thickness and permeability of cap rocks on CO_2 leakage was studied using a commercial compositional simulator. Experimental results show that the permeabilities of the shale samples measured by transient pulse technique range from 60 to 300 nD; a non-Darcy calibration factor which equals the ratio of the measured permeability divided by 1000, is identified for samples with permeability lower than 1000 nD. Numerical simulation results show that the largest leakage of CO_2 through the seal (cap cock) is about 7.0% with seal thickness of 3m and vertical permeability of 90 nD; both shale thickness and permeability affect the CO_2 leakage significantly; with a given seal permeability, the leakage rate has a power relationship with shale thickness.

Keywords: CO_2 storage, Cap rock properties, Permeability and thickness, CO_2 leakage.

1. INTRODUCTION

Injection of CO_2 into a confined geological formation is one of the most promising options for the long-term CO_2 storage and greenhouse gas mitigation (Bachu *et al*., 2007). The potential for CO_2 storage depends on the amount of CO_2 storage, carbon credit, and associated risks. Saline aquifers are considered to be the most important venue for CO_2 storage because they have the largest capacity compared with others, e.g. coal seam, depleted gas and oil fields (Nghiem *et al*., 2010). After injection, CO_2 is trapped in saline aquifers by mainly four mechanisms: structural trapping, residual gas trapping, solubility trapping and mineral trapping. Among these mechanisms, structural trapped CO_2 can flow and escape through the cap rock or sealing faults depending on their integrity (Nghiem *et al*., 2010).

A cap rock is usually a fine-grain lithology with low porosity and permeability such as shale. It forms a flow barrier to the migration of CO_2 and holds the CO_2 within the reservoir by virtue of the capillary pressure difference across the reservoir and seal boundary. The seal capacity is usually determined by its thickness, permeability and entry pressure (Schowalter, 1979; Downey, 1984; Vavra *et al*., 1992). Chiquet *et al*. (2005) reported, however, that the capillary pressure was altered in the presence of CO_2 under geological storage conditions because of the alteration of water-wettability of minerals. It is implicitly assumed in the definition of seal capacity that the CO_2 trapped beneath a seal can escape once its capacity is exceeded by the CO_2 column height. Such analysis, however, fails to recognize that CO_2 leakage is an extremely slow process of multiphase fluid flow due to the effects of viscosity and relative permeability through the low permeable cap rock. Siddiqui and Lake (1997) reported that viscous pressure drops are not negligible even at very low flow rates. Fisher *et al*. (2001) pointed out that if hydrocarbon charge into the reservoir is sufficient to keep the buoyancy force in the hydrocarbon column above the capillary entry pressure of the fault rock, hydrocarbon will leaks via the fault according to the Darcy's law. The leakage rate is governed by the relative hydrocarbon permeability of the fault rock and the hydrocarbon fluid pressures. As such, the current approach of seal assessment in terms of seal capacity can be quite conservative.

Rutqvist and Tsang (2002) studied the changes of cap rock hydro-mechanical properties in relation to injection of CO_2 into a brine formation. They reported that once the CO_2 reaches the upper part of the cap rock, through a permeable fault, migration of CO_2 is accelerated because of the combined effects of relative permeability and changes in viscosity and pressure-induced hydro-mechanical permeability. CO_2 migration and trapping of CO_2 can be considered as a gravity-driven multiphase fluid flow process where CO_2 displaces water and occupies structure highs. When a CO_2 column is thick and the capillary pressure of a seal is low, CO_2 starts to escape. This does not, however, mean that the seal is at immediate risk. Qualitatively, the effectiveness of a seal is determined by a number of factors: (1) buoyant force due to CO_2 column; (2) thickness and petrophysical properties, such as capillary pressure, absolute and relative permeability of seals; (3) the time period after the CO_2 column exceeds the seal capacity. A seal may be leaky, but trapped CO_2 may still exist over a significant period of time if the seal is relatively thick and extremely low permeability. This is due to the fact that it takes a long time for a significant portion of CO_2 to escape.

This paper examines the seal capacity by taking into account dynamic aspects of CO_2 leakage through seals as a function of time. Characteristics of fluid flow through extremely low permeability rocks are investigated experimentally by conducting flow tests on shale samples. A 3D compositional fluid flow model is adapted to simulate the process of CO_2 leakage through a top seal and compute the corresponding time-dependent CO_2 leakage as a function of cap rock thickness and permeability.

2. CAP ROCK SEALING MECHANISM

Most CO_2 accumulations in the subsurface are trapped by some kind of physical seal which prevents buoyancy-related upward migration. Watts (1987) presented a simple classification of seal types which are divided into cap rocks, faults and others, e.g. hydrodynamic seals. He pointed out that where CO_2 is trapped by a sealing fault a cap rock seal must also be present.

Apart from the case of seal failure due to high fluid pressure induced hydraulic fracturing, the dominant trapping mechanism is the capillary properties of cap rocks where the minimum displacement (or threshold, breakthrough) pressure of the cap rock equates to the pressure required to establish a connected CO_2 filament through the largest interconnected water-saturated pore throats (Schowalter, 1979). In other words, capillary force inhibits volume flow of a non-wetting CO_2 phase through a seal until the net buoyancy pressure of the underlying CO_2 exceeds the threshold capillary pressure of the cap rock seal. This mechanism has been considered as the major mechanism involved in stratigraphic trapping of CO_2 by Berg (1975) and the predominant trapping mechanism for cap rock seals by Schowalter (1979) and fault seals by Smith (1966; 1980).

Wardlaw *et al*. (1987; 1988) used percolation theory to describe the capillary sealing mechanism. Void spaces in porous media are considered as three-dimensional networks consisting of bulges (pores) connected by constrictions (throats). The degree of pore-throat size correlation affects fluid flow and displacement. During the displacement of wetting phase by non-wetting phase, as capillary pressure increased, smaller throats become invadeable with non-wetting phase until a point is suddenly reached at which a connected path of throats occupied by non-wetting phase extends through the media. This is referred as breakthrough.

A series of papers have discussed in detail the sealing efficiency of cap rock seals. It has been suggested that the maximum vertical CO_2 column trapped in a seal can be determined by using the following equation (Smith, 1966):

$$H_{\max} = \frac{Pd_B - Pd_R}{\rho_w - \rho_h} \tag{1}$$

where, H_{max} is the maximum vertical CO_2 column above the free water level before breakthrough occurs, Pd_B is subsurface CO_2-water displacement pressure of the sealing (boundary) bed, Pd_R is subsurface CO_2-water displacement pressure of the reservoir rock, ρ_w is subsurface density of water, ρ_h is subsurface density of CO_2. This

equation is widely used in studies of cap rock and fault sealing capacities (Smith, 1966; Berg; 1975, Schowalter, 1979; Zieglar, 1992; O'Connor, 2000). The density of supercritical CO_2 ranges from 0.42-0.74 g/cc and the water density from 0.97-1.05 g/cc with brine containing of 5000-65000 ppm (Daniel and Kaldi, 2008).

Reservoir rocks hosting CO_2 have different pore throat sizes and therefore have different threshold and displacement pressures (Daniel and Kaldi, 2008). The displacement pressure can be measured in the laboratory using mercury-air injection techniques and then converted to a CO_2-Brine system using Purcell's (1949) equation:

$$Pd_h = \frac{\sigma_h \cdot \cos\theta_h}{\sigma_m \cdot \cos\theta_m} \cdot Pd_m \tag{2}$$

where, Pd_h is capillary pressure for CO_2-water system, Pd_m is capillary pressure for mercury-air system, σ_h is interfacial tension of CO_2 and water under subsurface condition (Daniel and Kaldi, 2008; 27 mN/m), σ_m is interfacial tension of mercury and air (480 mN/m), θ_h is contact angle of CO_2 and water (assumed to be 0º for wetting phase; Daniel and Kaldi, 2008), θ_m is contact angle of mercury and air against the rock (130°).

The seal capacity is therefore a function of fluid densities, displacement pressure and the CO_2/water interfacial tension at subsurface conditions. Mercury capillary curves are usually used to determine displacement pressure, which is critical in estimating CO_2 seal capacity as seen in Eq. 1. In estimating displacement pressures from capillary pressure curves, it has been assumed that a continuous non-wetting filament would occur somewhere on the capillary pressure curves. The problem here is how to locate the point of occurrence of a continuous non-wetting filament on the capillary pressure curve.

Different approaches exist in the literature regarding to the determination of displacement pressure. In the first approach, displacement pressure is estimated by extending the slope of the "plateau" of the capillary pressure curve to the logarithmic pressure axis (Fig. 1) (Schowalter, 1979; Jennings, 1987). This approach, as pointed out

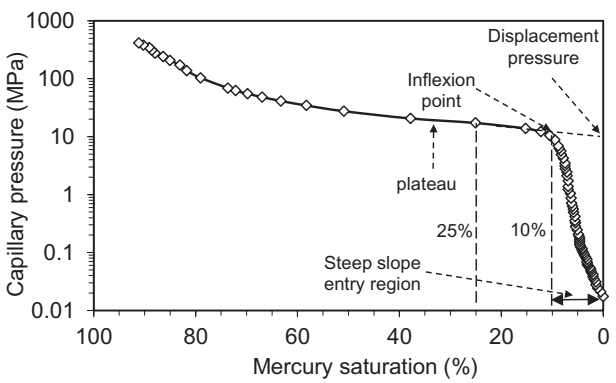

Figure 1. Capillary pressure curve of Muderong shale for mercury-air system.

by Schowalter (1979), seems quite adequate where the capillary plateau is nearly flat. However, for rocks with steep capillary plateaus or no plateau, the displacement pressure cannot be accurately estimated by this approach. Chatzis and Dullien (1981) denoted that the displacement pressures estimated by this empirical method are always less than the true values by an amount depending on the nature of the sample and its size.

In the second approach, displacement pressure is estimated as the pressure corresponding to the critical non-wetting phase saturation (breakthrough saturation) on the capillary pressure curve. The breakthrough saturation is determined by conducting fluid injection experiments. Schowalter (1979) performed capillary breakthrough experiments with nitrogen and mercury on samples of sandstone, chalk and silty shale. The non-wetting phase saturation is needed to establish a connected filament across the length of the samples which ranged from 4.5% to 17% of the rock pore volume. Based on the experimental results, Schowalter (1979) suggested that displacement pressures could be estimated from standard mercury capillary pressure curves by determining the mercury pressure on the capillary curve at 10% mercury saturation. Chatzis and Dullien (1981) performed unidirectional mercury breakthrough experiments on sandstone samples. The mercury breakthrough was detected by making electrical conductivity readings during mercury injection. The saturation at the breakthrough was found to lie in the range of 10%-25%. Although the above breakthrough experiments were performed mainly on sandstone samples, it is obvious that the saturations at breakthrough for different samples vary in a wide range of 4.5%-25%. It is, therefore, difficult to estimate the true breakthrough saturation and displacement pressure for a specific rock sample without direct measurement.

A third approach to the determination of displacement pressure combines the direct measurement of the pressure and saturation at breakthrough with the characteristics of the mercury capillary curves. Katz and Thompson (1986; 1987) indicated that the measured threshold pressure corresponded graphically to the inflection point on a mercury injection capillary pressure curve (Fig. 1). Chatzis and Dullien's (1981) experiments showed a similar result. Physically, the inflection point marks the pressure at which the incremental rate of intrusion of mercury with increasing pressure is highest and in terms of pore size distribution, it represents the most prominent pore radius (Schlomer and Krooss, 1997). This approach seems to work well for sandstone, but there is not enough experimental evidence to validate the method in the case of shale. Nevertheless, this approach has been used by many people in the analysis of seal capacity (Kaldi, 2000; Jones, 2000; Dragomirescu, 2000).

As discussed above, different approaches may give quite different values of displacement pressure for a same capillary curve, which may result in significant discrepancies in evaluating sealing capacity. To illustrating this effect, the capillary pressure curve of Muderong shale (Fig. 1), is considered in this study. Pressures at 10%, 25% of mercury saturation and at inflection point are taken to evaluate the sealing capacity. The results and the parameters required in the calculation are presented in table 1. It can be seen from this table that the seal capacity values calculated for different points on capillary pressure curve (10%, 25% of mercury saturation and at inflection point) vary significantly. In addition, simulation results presented in the results section demonstrate that the displacement pressure calculated

Table 1. Sealing capacity of Muderong shale.

Displacement pressure (MPa) by Mercury-air system	Seal capacity (m) for CO_2
9.65 (10% mercury saturation)	174
12.19 (inflexion point)	225
17.21 (25% mercury saturation)	325
Parameters used in seal capacity calculations with Eqs. (1) and (2):	
Density: ρ_w=1.05g/cc; $\rho_{h(CO2)}$ = 0.6g/cc;	
Interfacial tension: $\sigma_{h(CO2)}$ = 27 mN/m; $\sigma_{m(mercury)}$= 480 mN/m;	
Contact angle: $\theta_{h(CO2\text{-}water)}$ = 0°; $\theta_{m(mercury\text{-}air)}$= 130°;	

using these different approaches have significant influence on the rate of CO_2 leakage through seals.

Note that for complex heterogeneous lithologies, in particular for laminated, anisotropic lithologies, displacement pressure obtained from omnidirectional (uncoated sample) mercury intrusion measurements is not sufficient to characterise capillary sealing efficiency. A more reliable assessment of the sealing efficiency would require unidirectional (coated sample) measurements at high-pressure levels. Wardlaw and Taylor (1976) pointed out that measurement on uncoated samples usually yields a lower displacement pressure than coated samples due to the effects of invasion of surface spaces.

Once the displacement capillary pressure of the seal is exceeded by the net buoyancy pressure, the underlying CO_2 will leak through the seal in the form of multiphase fluid flow (Schowalter, 1979; England *et al*., 1987; Ingram *et al*., 1997; Kettel, 1997; Siddiqui and Lake, 1997; Brown, 2000). Quantitative analysis of CO_2 leakage through cap rock seals has not been carried out (Schlomer and Krooss, 1997).

3. MULTIPHASE FLUID FLOW SIMULATION IN CAP ROCKS

Multiphase fluid flow through porous media can be represented mathematically by a set of partial differential equations. Under isothermal conditions, these governing differential equations as listed below can be derived from mass conservation and Darcy's law (Aziz and Settari, 1979):

$$\frac{\partial(\varphi\rho_w S_w)}{\partial t}+\nabla\cdot(\rho_w v_w)+q_w=0 \tag{3}$$

$$\frac{\partial(\varphi\rho_n S_n)}{\partial t}+\nabla\cdot(\rho_n v_n)+q_n=0 \tag{4}$$

$$v_w=-\frac{kk_{rw}}{\mu_w}(\nabla p_w-\rho_w g\nabla D) \tag{5}$$

$$v_n = -\frac{kk_{rn}}{\mu_n}(\nabla p_n - \rho_n g \nabla D) \tag{6}$$

$$p_c(S_w) = p_n - p_w \tag{7}$$

$$S_w + S_n = 1 \tag{8}$$

where v is the fluid flow velocity, k and k_r are the absolute and relative permeability respectively, μ is the viscosity, p_c is the capillary pressure, p is the pressure, S is the saturation, q is the mass flow rate of production or injection fluid, subscript w and n represent wetting phase and non-wetting phase respectively.

When solving Eqs. 3 to 8 numerically, one can obtain pressures and saturations of each phase. Currently, many numerical solutions have been developed based on Eqs. 3 to 8, however, in this study a compositional simulator was used because it has been widely used in reservoir simulations and is readily available.

It should be noted that to solve the above equations, reliable petrophysical and fluid transport parameters for the various lithologies encountered in the CO_2 systems must be available. There is, however, little information available on tight seal lithology (such as the cap rock shale), specifically the absolute permeability and the relative permeability, because most of the works on fluid flow in porous media have been carried out for permeable sandstones. Similarly, the methodology of numerical simulation of fluid flow in porous media has been well established for sandstone reservoirs. Its applicability to fluid flow in shale is unknown. Therefore, in this study, absolute permeability and relative permeability of shale are characterized through laboratory experiments, and the multiphase fluid flow process through shale is investigated experimentally. These experimental results are used to verify the applicability of the numerical simulator in the simulation of CO_2 leakage through cap rock seals.

4. EXPERIMENTAL INVESTIGATION OF FLUID FLOW IN SHALES

4.1. Collection and preparation of shale samples

Natural shale samples were collected from Hudson, Muderong (a major top seal in the Carnarvon Basin, North West Shelf, Australia) and Wanea formations to measure permeability, porosity and pore size distribution (pore entry diameter distribution). Synthetic shale samples were used to study fluid flow characteristics in order to eliminate the effect of chemical potential of natural shale on the fluid flow behavior (Rahman *et al*., 2005). Two synthetic shales, Johnstone I and Johnstone II were prepared according to the procedure by Johnston and Choi (1986), by which pore size distribution and permeability of the synthetic shale were controlled to resemble a range of natural shales (Hudson, Muderong, Wanea, etc.) with sufficient accuracy.

4.2. Determination of shale permeability

Absolute permeability measurement of low permeability rocks, such as the shales by conventional steady-state method is generally impractical or difficult, because a long

time is required to establish a steady state fluid flow. To overcome this problem, unsteady-state method was used to measure permeability of tight rocks (Jones, 1972; Freeman and Bush, 1983; Zeynaly-Andabily and Rahman, 1995). Furthermore the unsteady-state methods produce a more consistent permeability than steady-state methods. The experimental results of Freeman and Bush (1983) shows that the permeability values measured using unsteady-state method normally differ by less than 5% from those obtained by steady state methods.

In this study, a transient pulse technique developed by Zeynaly-Andabily and Rahman (1995) was used to measure permeability of the shale samples. The transient pressure pulse apparatus consists of a core holder, which houses a cylindrical rock sample and allows application of radial and axial pressure, and instrumentation to apply and record confining, upstream and downstream pressures. The core sample is connected to upstream and downstream fluid reservoirs at the two ends. High precision pressure transducers are used to accurately measure the pressures along the length of the sample. The whole transient pressure pulse apparatus is housed in an oven for maintaining a constant temperature during the experiment. The pressures are monitored and recorded by a data acquisition system. During an experiment the core sample was first saturated with a simulated pore fluid (brine) and maintained at a constant pore pressure to achieve equilibrium condition. Due to the very low permeability of shale, saturation of testing sample takes two to four weeks till pressures at the measuring ports along the rock sample and at the inlet and outlet ends are stabilized. At the beginning of an experiment, the fluid pressure in the upstream reservoir is increased (pulse). As the fluid flows from the upstream reservoir, across the sample, to the downstream reservoir, the pressure in the upstream reservoir diminishes. The permeability of the rock sample was determined by matching measured pressure decay at the upstream reservoir with those generated using numerical simulations. For details readers are referred to publication, Zeynaly-Andabily and Rahman (1995).

4.3. Determination of relative permeability for shale samples

Relative permeability is a measure of hydrodynamic conductance of each fluid when two or more phases are present and is defined as a ratio of the effective to absolute permeability for each phase. It is independent of flow rate and fluid properties, but is dependent upon fluid saturation. Relative permeability can be determined using either steady-state or unsteady-state methods. The relative permeability curves for shale is difficult to obtain through laboratory measurements due to the extremely low absolute permeability. The relative permeability curves in this study are constructed using a modified Corey's model (van Golf-Racht, 1982).

According to Corey's method, the relative permeability under drainage condition for wetting and non-wetting phases are expressed as:

$$k_{rwt} = (S_{wt}^{*})^{\frac{2+3\lambda}{\lambda}} \tag{9}$$

$$k_{rnwt} = (1 - S_{wt}^{*})^{2}\left(1 - (S_{wt}^{*})^{\frac{2+\lambda}{\lambda}}\right) \tag{10}$$

where, k_{rwt} and k_{rnwt} are wetting and non-wetting phase relative permeability, S_w and S_{nw} are wetting and non-wetting phase saturations respectively, λ is pore size distribution index, and S_{wt}^* is normalized wetting phase saturation and defined as:

$$S_{wt}^* = \frac{S_w - S_{wc}}{1 - S_{wc}} \tag{11}$$

where, S_{wc} is residual wetting phase saturation which can be determined from the drainage capillary pressure-saturation curve from mercury injection capillary pressure test.

The capillary pressure can be expressed as a function of normalized wetting phase saturation:

$$\log P_c = \log P_{co} - 1/\lambda \log S_{wt}^* \tag{12}$$

where, P_{co} is capillary pressure at $S_{wt} = 1$.

The distribution index λ and P_{co} can be obtained by matching the measured capillary pressure curve using Eq. 12. Small values of λ indicate a wide distribution of pore sizes while a large λ means uniformity in pore size. The average pore size mainly influences the value of P_{co}.

4.4. Experiment of fluid flow through shale samples

The experimental investigation of fluid flow through shale was carried out in the laboratory by using pressure penetration test equipment. The pressure penetration test equipment consists of a core-holder with multi pressure ports for measuring the pressures along the length of core sample. Figure 2 gives a schematic of the pressure penetration test equipment.

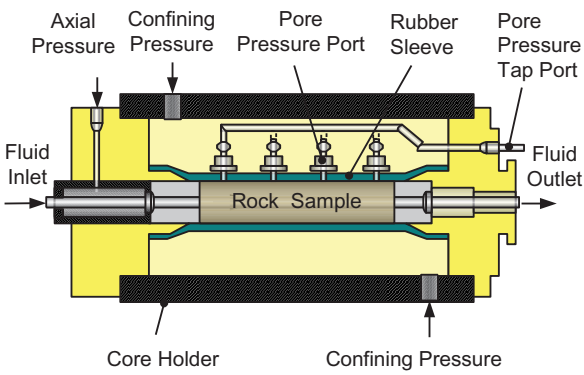

Figure 2. Schematic diagram of pressure penetration test equipment.

A shale sample of 2.5 cm in diameter and up to 20 cm in length was mounted in the core holder and confining and axial pressures were applied. The core sample was first saturated with a simulated pore fluid (brine) and maintained at a constant pore pressure. Then the sample was exposed to pressurized fluid at the upstream end and a differential pressure was established and maintained in the same level during the test. Changes in pore pressure with time at different positions along the core length were recorded continuously by a multi-tap pressure transducer system. The effluent fluid displaced out from the sample was collected at the downstream reservoir.

5. RESULTS AND DISCUSSION

5.1. Mercury injection tests results

The pore size distributions obtained from mercury injection (MICP) tests of two synthetic shales (Johnstone I and Johnstone II) and two natural shales (Muderong and Wanea) are given in figures 3 and 4. It can be seen from these figures that Johnstone I has a similar pore size distribution to that of Muderong shale, and Johnstone II to that of Wanea shale.

5.2. Permeability and relative permeability

The permeability of samples from natural shale Muderong, Wanea and Hudson and synthetic shale Johnstone I and II were measured. Table 2 listed all the history matched permeability for the samples. Results show that measured permeability of shale sample Muderong, Hudson and Wanea are 300 nD, 120 nD and 60 nD, respectively, while the permeability of Johnstone I and II are 1470 and 100 nD, respectively.

Table 2. Shale permeability measured using pulse technique at a confining pressure of 10.5 MPa (1500psi).

Shale	Permeability, nD
Johnstone I	1470
Johnstone II	100
Wanea	60
Hudson	120
Muderong	300

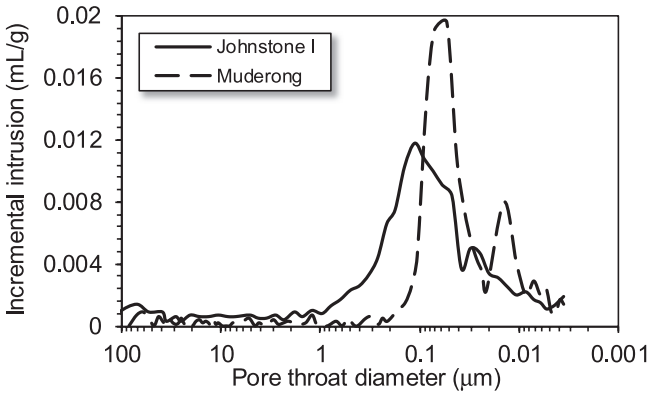

Figure 3. Pore size distributions of Johnstone I and Muderong shale (from MICP test).

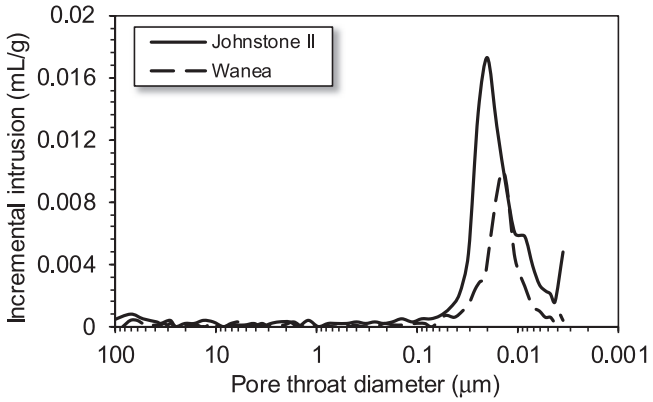

Figure 4. Pore size distributions of Johnstone II and Wanea shale (from MICP test).

The capillary pressure curve obtained from mercury injection capillary pressure (MICP) test for Muderong shale sample is presented in figure 1. By matching the measured capillary pressure curve using Eq. 12, the pore size distribution index (λ) is found to be 0.95 (Fig. 5). Note that the capillary pressure curve obtained from MICP test has been converted to CO_2-water system under subsurface conditions using Eq. 2. The same procedure has been applied to Johnstone I, Johnstone II and Wanea shale samples, and the pore size distribution indices (λ) are found to be 0.805, 1.32 and 1.48, respectively.

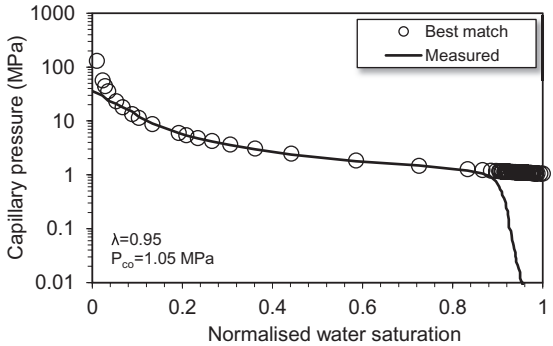

Figure 5. Capillary pressure matching for Muderong shale of water-CO_2 system.

The relative permeability for wetting and non-wetting phases is determined from Eqs. 9 and 10, respectively. Figure 6 presents relative permeability curves as a function of normalised wetting phase saturation for Muderong shale. The relative permeability curves for Johnstone I and Johnstone II are also obtained using the same procedure. In this study, the relative permeability curves of Muderong shale were used in the simulations.

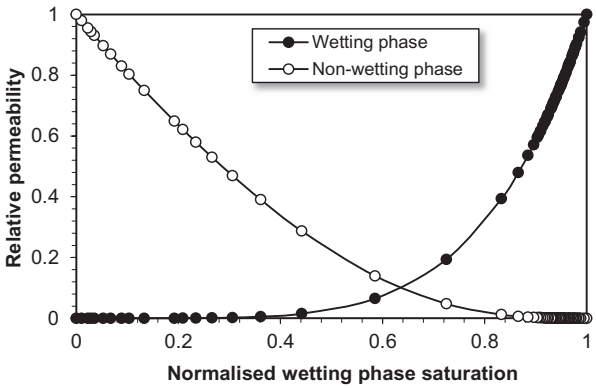

Figure 6. Relative permeability curves of Muderong shale.

5.3. Permeability calibration factors

A series of pressure penetration experiments were carried out in order to understand the change in pore pressure due to fluid penetration in tight rocks. The first series of tests were conducted on Johnstone I samples of a measured permeability of 1470 nD. The fluid flow process through cores was also simulated using a black oil simulator. An example of comparison between the pore pressure estimated by the numerical model and that obtained experimentally is shown in figure 7. In this test, the virgin core with a length of 20 cm was used and a differential pressure of 2.2 MPa was maintained

at sample ends. As can be seen from figure 7, the numerical results match satisfactorily with the experimental data for this relatively permeable synthetic shale.

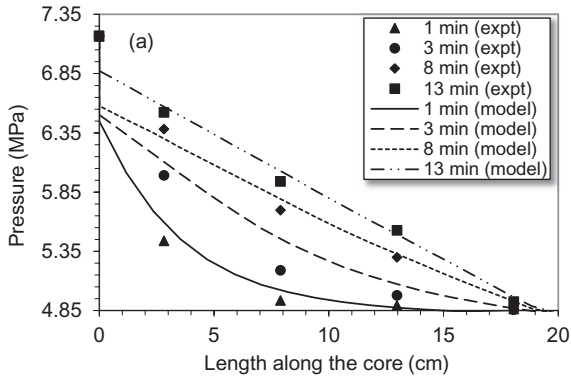

Figure 7. Experimental and simulated pressure profiles of Johnstone I shale (expt=experiment).

Another series of tests were carried out on Johnstone II samples. Figure 8 compares the experimental and numerical results. As can be seen from this figure, pore pressures predicted by the model are much higher than the experimental results. Possible explanations for this discrepancy are that the flow characteristic in extremely low permeable Johnstone II shale (around 100 nD) is of non-Darcy nature. However, by introducing a calibration factor of 0.1 to the absolute permeability, it is possible to obtain a reasonable match (Fig. 9). This implies that by introducing a calibration factor to the permeability, the current numerical model can be used to simulate multiphase fluid flow through low permeable shales.

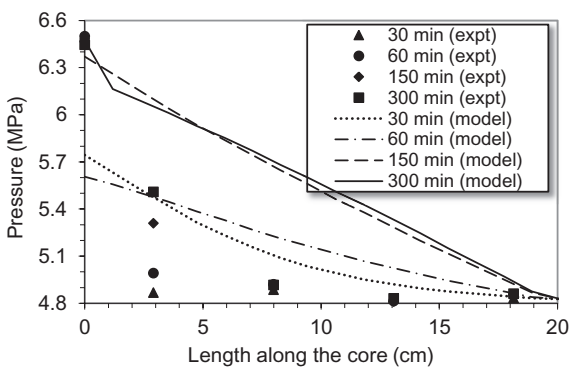

Figure 8. Experimental and simulated pressure profiles in Johnstone II shale (expt=experiment).

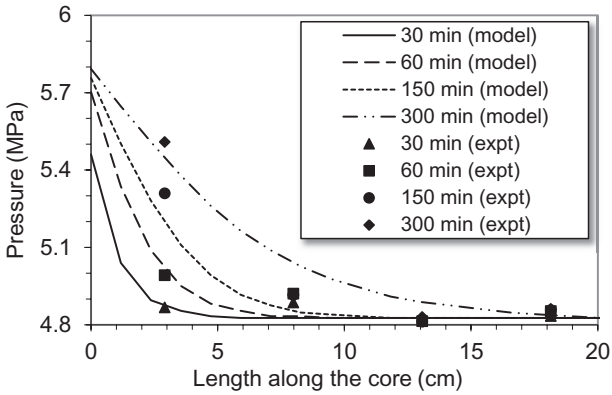

Figure 9. Experimental and simulated pressure profiles in Johnstone II shale after applying a calibration factor of 0.1 to the permeability (expt=experiment).

5.4. Model Setup for simulation of CO_2 leakage

A 3D middle seal model as described in figure 10 is used in this study. This model represents a vertical slice of the seal-reservoir system. Dimensions of the model along x- and y-direction are 2000 m. The thicknesses of upper and lower aquifers are 100 m and 400 m respectively. The grid size in x- and y- direction is 50 m. The shale thicknesses are assigned as 24 m, 12 m, 6 m and 3 m for different cases which gridded into 3 layers, respectively. The porosity and horizontal permeability for both upper and lower aquifers are 30% and 1000mD. The porosity of shale is 1%. The horizontal permeability is 10 times than its vertical ones for the entire model. Note that in this study a modified Darcy's law is used to simulate fluid flow in shale by applying a permeability calibration factor to rocks having permeabilities less than 1000 nD. Based on the experiment results of Johnstone I and II, the permeability calibration factor is determined by K/1000, where K is the permeability of shale in nD. Note that permeability calibration factor (K/1000) is determined from limited experimental data and more investigation need to be conducted. While for rocks having permeabilities greater than 1000 nD, no permeability calibration factor is applied. The measured permeabilities, 300 nD, 120 nD and 60 nD, for the three samples are considered as

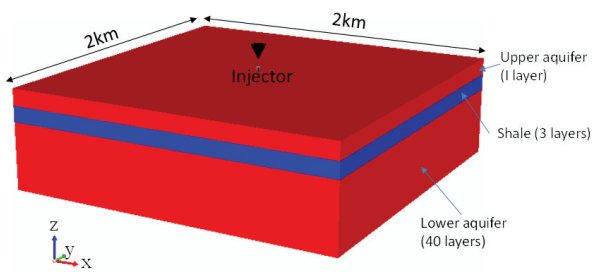

Figure 10. 3D Reservoir model for numerical simulation.

vertical permeability. Hence the horizontal permeability of 600 nD was calibrated to 360 nD and the three vertical permeabilities, 300 nD, 120 nD and 60 nD were calibrated as 90 nD, 15 nD and 4 nD, respectively. Table 3 lists all the reservoir properties for the 12 scenarios.

The model was then discretized into 40 cells in x- and y- directions and 44 layers vertically. The injection well penetrates in to the bottom grid. Li *et al*. (2012) reported that Brooks-Corey-type (BC-type; Brooks and Corey, 1964) model uses a plateau that ends with a nonzero capillary entry pressure, while the van Genuchten-type (VG-type; van Genuchten, 1980) model uses an entry region, and the amount of dissolved CO_2 simulated with VG-type model can be twice as larage as that with BC-type. In this study, VG-type model with a steep slope entry region is used. The aquifer and shale are assigned with different dynamic properties of capillary pressure (Fig. 11). The relative permeability for shale and aquifer are described in figures 6 and 12, respectively.

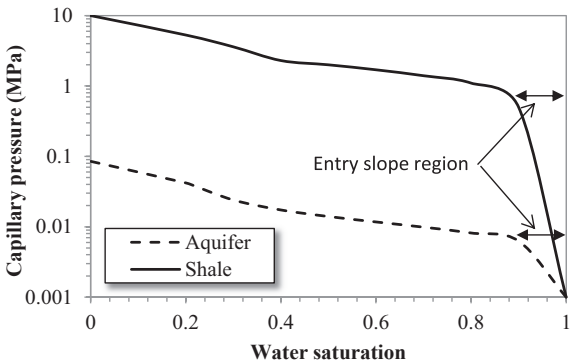

Figure 11. Capillary pressure curves for aquifers and shale used in simulation.

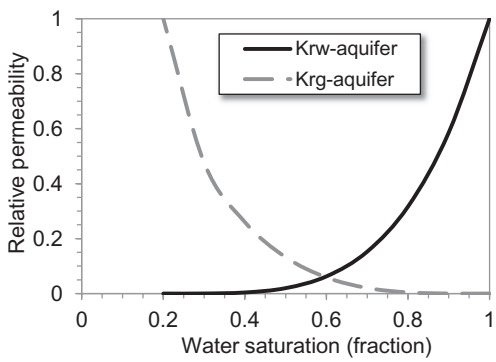

Figure 12. Relative permeability for CO_2 and brine in aquifers (after Mo and Akervoll, 2005).

The reservoir is initialized with gravity-capillary equilibrium method with reference pressure of 10MPa at reference depth of 1000m which is the top depth of the model. Note that CO_2-brine-rock interactions is not simulated because our aim is focused on the seal capacity of cap rock instead of a traditional assessment of CO_2 storage (Pruess and Garcia, 2002) which simulates all the structural trap, residual gas trapping, solubility trapping and mineral trapping.

Then CO_2 is injected at a constant pressure of 50 MPa for 50 years through the bottom grid. The numerical simulation runs for more 1000 years after stop injection.

Table 3. Properties in different scenarios.

Scenarios	Shale horizontal permeability (nD)*	Shale vertical permeability (nD)		Shale Thickness (m)	Shale Porosity (%)
		Calibrated	Measured		
S_1	3000	90	300	24	1
S_2	3000	90	300	12	1
S_3	3000	90	300	6	1
S_4	3000	90	300	3	1
S_5	1200	15	120	24	1
S_6	1200	15	120	12	1
S_7	1200	15	120	6	1
S_8	1200	15	120	3	1
S_9	360 **	4	60	24	1
S_{10}	360**	4	60	12	1
S_{11}	360 **	4	60	6	1
S_{12}	360 **	4	60	3	1

Note: *-10 times the measured permeability; **- calibrated from 600 mD.

5.5. Effect of cap rock permeability and thickness on leakage

The storage volume of the CO_2 at standard condition (1 atm, 25 ˚C) are calculated using following equation:

$$V_S = \frac{P_R V_R Z_S T_S}{Z_R P_S T_R} \tag{13}$$

where, P, V, Z and T are pressure, volume, compressibility and temperature respectively, subscripts R and S represent reservoir condition and standard condition respectively.

In this study we assumed that the reservoir temperature keeps constant. The CO_2 compressibility is calculated by Soave-Redlich-Kwong equations of state (Zhou *et al*., 2013). Injection of CO_2 begins in 2012 and continued over a period of 50 years. Total volume of CO_2 injected for different scenarios ranges from 371×10^9 m^3 to 377×10^9 m^3 at standard condition. The leakage volume of CO_2 in upper aquifer, middle shale section and lower aquifer at standard condition for each time step is calculated using Eq. 13. The rate of leakage is calculated based on leakage volume of CO_2 at standard condition in the upper aquifer divided by the total injected volume of CO_2 at the end of 2062 at standard condition.

In figure 13 the gas saturation at the end of injection, 2062 is presented. From the figure it can be seen that gas saturation near the injection point is higher and decrease outward. In figure 14 the percentage of CO_2 leakage with time for all 12 scenarios is presented. From the figure it can be seen that CO_2 leaked through the seal to the upper aquifer for scenarios S_1, S_2, S_3, S_4, S_6, S_7, S_8, S_{11}, and S_{12} by the time injection has completed in 2062 with S_4 exhibiting highest rate of leakage (total of 26.5×10^9 Sm^3 CO_2). This is because that the shale vertical permeability of S_4 is highest while its shale thickness is thinnest. Scenario S_9 has been found to be the most effective in containing CO_2 for having thickest shale and low vertical permeability. For scenario S_9, CO_2 begins to leak through the seal in 2262, which is 200 years after the completion of injection, and a total of 0.5×10^9 Sm^3 of CO_2 leaked into the upper aquifer at the end of 1000 years.

Figure 15 shows the relationship between the CO_2 leakage percent with shale thickness for three different shale vertical permeabilities. Results show that if the permeability of seal is kept constant the leaked volume (in percentage) of CO_2 has a power-relationship with shale thickness. It can also be seen that with decreasing the seal permeability the correlation coefficient increases. For membrane seals, however, the seal layer thickness has been found to have less effect on CO_2 leakage because the property that controls CO_2 leakage is the capillary entry pressure of the largest interconnected pore throat (Nelson *et al*., 2005). Saadatpoor *et al*., (2010) also reported that the thickness of seal layer does not affect the leakage volume if an active open aquifer is present. Figure 16 shows the relationship between the CO_2 leakage percent with shale vertical permeabilities. Results show that the total leakage percent at 3062 is logarithmic with shale vertical permeability if the shale thicknesses are 24 and 12 m. For scenarios with shale thicknesses of 3 and 6 m, the total leakage percent at 3062 increase linearly with shale vertical permeability.

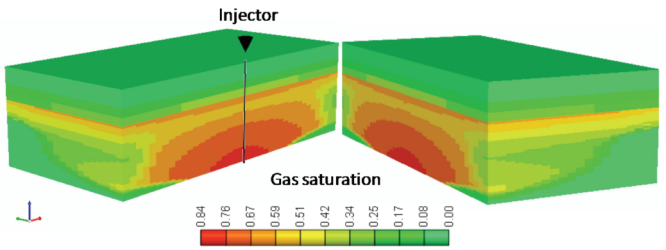

Figure 13. Gas saturation at the end of injection of 2062.

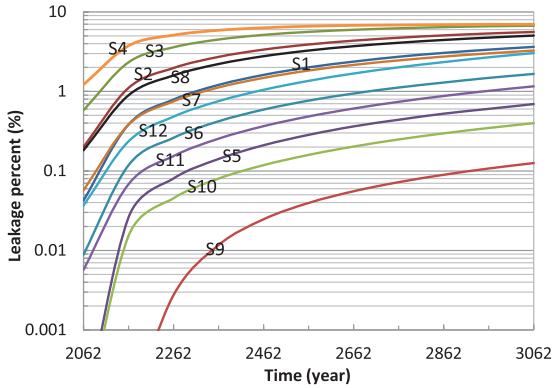

Figure 14. Leakage percentage against the time of the all 12 scenarios.

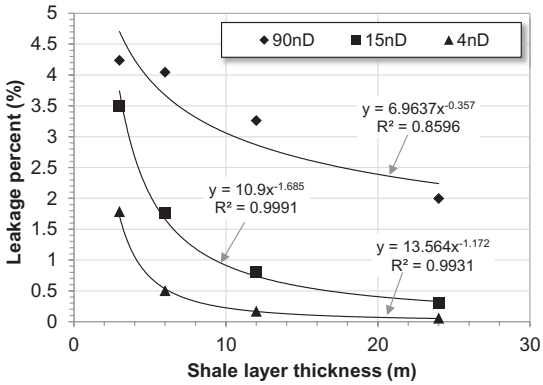

Figure 15. Relationship between leakage percentages of total sequestrated CO_2 and shale thickness with shale permeability of 90, 15 and 4 nD, respectively.

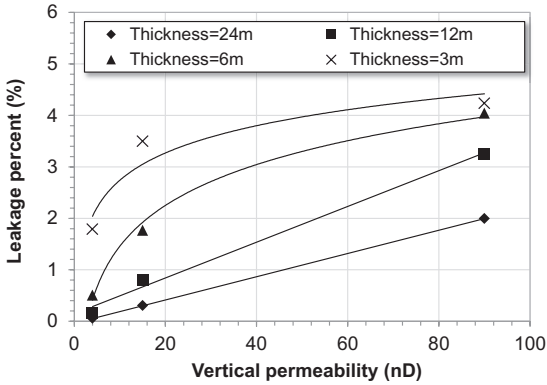

Figure 16. Relationship between leakage percentages of total sequestrated CO_2 and shale vertical permeability with shale thickness 24, 12, 6 and 3 m, respectively.

6. CONCLUSIONS

This paper investigates the effects of CO_2 leakage through cap rock seal by combining experimental studies and numerical simulations. We determined the capillary pressure, pore size distribution and permeability of Australian shale samples in laboratory. Then we studied the effects of thickness and permeability of cap rocks on CO_2 leakage using a compositional simulator. Following conclusions are drawn:

1. Transient pulse technique is efficient to determine the permeability for shale samples. Results show that shale sample # Muderong has highest permeability of 300 nD, then Hudson of 120 nD and Wanea of 60 nD. A non-Darcy calibration factor (measured permeability over 1000) is found for samples with permeabilities less than 1000 nD.
2. Both shale thickness and shale vertical permeability affect the leakage percent of CO_2. The largest leakage percent is approximately 7.0% with shale thickness of 3 m and calibrated shale vertical permeability of 90 nD in 1000 years after CO_2 injected.
3. The leakage percentage of CO_2 has a power-relationship with shale thickness if they have same shale vertical permeability.

ACKNOWLEDGEMENTS

The Author thanks the Computer Modelling Group for providing the compositional simulator GEM™ for this study.

REFERENCES

Aziz K. and Settari A., 1979. Petroleum Reservoir Simulation. Applied Science Publishers. London.

Bachu S., Bonijoly D., Bradshaw J., Burruss R., Holloway S., Christensen N.P. and Mathiassen O.M., 2007. CO_2 storage capacity estimation: methodology and gaps. *International Journal of Greenhouse Gas Control* **1(4)**, 430-443.

Berg R.R., 1975. Capillary pressure in stratigraphic traps. *The American Association of Petroleum Geologists Bulletin* **59(6)**, 939-956.

Brooks R.H. and Corey A.T., 1964. Hydraulic properties of porous media. Colorado State University, Fort Collins, Colorado.

Brown A., 2000. Evaluation of possible gas microseepage mechanisms. *The American Association of Petroleum Geologists Bulletin* **84(11)**, 1775-1789.

Chatzis I. and Dullien F.A.L., 1981. Mercury porosimetry curves of sandstones. Mechanisms of mercury penetration and withdrawal. *Power Technology* **29(1)**, 117-125.

Chiquet P., Broseta D.F. and Thibeau S., 2005. Capillary alteration of shaly caprocks by carbon dioxide. SPE Europec/EAGE Annual Conference, Madrid, Spain, June 13-16, 2005.

Daniel R.F. and Kaldi J.G., 2008. Evaluating seal capacity of caprocks and intraformational barriers for the geosequestration of CO_2. In: Blevin B.E. Bradshaw and Uruski C. (Eds.). Third Eastern Australasian Basins Symposium: EABS III: energy security for the 21st century/J.E. Petroleum Exploration

Society of Australia, Sydney, Australia, Setember 14-17, 2008, pp. 475-484.

Downey M.W., 1984. Evaluating seals for CO_2 accumulations. *The American Association of Petroleum Geologists Bulletin* **68(11)**, 1752-1763.

Dragomirescu R., 2000. Triassic seals in the Cooper Basin, CO_2 Sealing Potential of Faults and Cap Rocks. Technical Workshop Proceedings, McLaren Vale, Australia, November 5-7, 2000.

England W.A., Mackenzie A.S., Mann D.M. and Quigley T.M., 1987. The movement and entrapment of petroleum fluids in the subsurface. *Journal of the Geological Society* **144(2)**, 327-347.

Fisher Q.J., Harris S.D., McAllister E., Knipe R.J. and Bolton A.J., 2001. Hydrocarbon flow across faults by capillary leakage revisited. *Marine and Petroleum Geology* **18(2)**, 251-257.

Freeman D.L. and Bush D.C., 1983. Low-permeability laboratory measurements by nonsteady-state and conventional methods. *Society of Petroleum Engineers Journal* **23(6)** 928-936.

van Golf-Racht T.D., 1982. Fundamentals of fractured Reservoir Engineering. Elsevier Science Publisher, New York.

Ingram G.M., Urai J.L. and Naylor M.A., 1997. Sealing processes and top seal assessment, In: Moller-Pedersen P. and Koestler A.G. (Eds.), CO_2 Seals: Importance for Exploration and Production, New Petroleum Society Special Publication 7. Elsevier, Singapore, pp. 165-174.

Jennings J.B., 1987. Capillary pressure techniques: application to exploration and development geology. *The American Association of Petroleum Geologists Bulletin* **71(10)**, 1196-1209.

Jones R.M., 2000. Quantitative fault seal risking: An integrated approach to reducing fault seal uncertainty, CO_2 Sealing Potential of Faults and Cap Rocks. Technical Workshop Proceedings, McLaren Vale, Australia, November 5-7, 2000.

Jones S.C., 1972. A rapid accurate unsteady-state Klinkenberg permeameter. *Society of Petroleum Engineers* **12(5)**, 383-397.

Kaldi J.G., 2000. Evaluating the CO_2 sealing potential of faults and cap rocks, CO_2 Sealing Potential of Faults and Cap Rocks. Technical Workshop Proceedings, McLaren Vale, Australia, November 5-7, 2000.

Katz A.J. and Thompson, A.H., 1986. Quantitative prediction of permeability in porous rock. *Physical Review B* **34 (11)**, 8179-8181.

Katz A.J. and Thompson A.H., 1987. Prediction of rock electrical conductivity from mercury injection measurements. *Journal of Geophysical Research* **92(B1)**, 599-607.

Kettel D., 1997. The dynamics of gas flow through rock salt in the scope of time. In: Moller-Pedersen P. and Koeslter A.G. (Eds.), CO_2 Seals: Importance for Exploration and Production, Norwegian Petroleum Society Special Publications 7. Elsevier, Singapore, pp. 175-185.

Li B., Tchelepi H.A. and Benson S.M., 2012. The influence of capillary entry-pressure representation on the rate of CO_2 solubility trapping. Proceedings, Tough

Symposium, Lawrence Berkeley National Laboratory, Berkeley, California, September 17-19, 2012. pp. 1-8.

Mo S. and Akervoll I., 2005. Modeling long-term CO_2 storage in aquifer with a Black-oil reservoir simulator. Society of Petroleum Engineers, 2005. SPE/EPA/DOE Exploration and Production Environmental Conference, Galveston, Texas, USA, March 7-9, 2005.

Nelson C.R., Evans J.M., Sorensen J.A., Steadman E.N. and Harju J.A., 2005. Factors affecting the potential for CO_2 leakage from geologic sinks. Plains CO_2 Reduction (PCOR) Partnership, Practical, Environmentally Sound CO2 Sequestration. Energy & Environmental Research Center, pp. 36.

Nghiem L., Shrivastava V., Kohse B., Hassam M. and Yang C., 2010. Simulation and optimization of trapping processes for CO_2 storage in saline aquifers. *Journal of Canadian Petroleum Technology* **49(8)**, 15-22.

O'Connor S.J., 2000. Hydrocarbon-water interfacial tension values at reservoir conditions: Inconsistencies in the technical literature and the impact on maximum oil and gas column height calculations. *The American Association of Petroleum Geologists Bulletin* **84(10)**, 1537-1541.

Pruess K. and Garcia J., 2002. Multiphase flow dynamics during CO_2 disposal into saline aquifers. *Environmental Geology* **42(2-3)**, 282-295.

Purcell W.R., 1949. Capillary pressure-their measurements using mercury and the calculation of permeability therefrom. *Journal of Petroleum Technology* **1(2)**, 39-48.

Rahman M.M., Chen Z. and Rahman S.S., 2005. Experimental investigation of shale membrane behavior under tri-axial conditions. *Petroleum Science and Technology* **23 (9-10)**, 1265-1282.

Rutqvist J. and Tsang C.F., 2002. A study of caprock hydromechanical changes associated with CO_2-injection into a brine formation. *Environmental Geology* **42(2-3)**, 296-305.

Saadatpoor E., Bryant S.L. and Sepehrnoori K., 2010. CO_2 leakage from heterogeneous storage formations. SPE Annual Technical Conference and Exhibition, Florence, Italy, September 19-22, 2010.

Schlomer S. and Krooss, B.M., 1997. Experimental characterization of the CO_2 sealing efficiency of cap rocks. *Marine and Petroleum Geology* **14(5)**, 565-580.

Schowalter T.T., 1979. Mechanics of secondary CO_2 migration and entrapment. *The American Association of Petroleum Geologists Bulletin* **63(5)**, 723-760.

Siddiqui F.I. and Lake L.W., 1997. A comprehensive dynamic theory of CO_2 migration and trapping. SPE 72nd Annual Technical Conference & Exhibition, San Antonio, Texas, October 5-8, 1997.

Smith D.A., 1966. Theoretical consideration of sealing and non-sealing faults. *The American Association of Petroleum Geologists Bulletin* **50(2)**, 363-374.

Smith D.A., 1980. Sealing and non-sealing faults in Louisiana Gulf Coast Basins. *The American Association of Petroleum Geologists Bulletin* **64(2)**, 145-172.

Vavra C.L., Kaldi J.G. and Sneider R.M., 1992. Geological applications of capillary pressure: A review. *The American Association of Petroleum Geologists Bulletin* **76(6)**, 840-850.

Genuchten van M.T., 1980. A closed-form equation for predicting the hydraulic conductivity of unsaturated soils. *Soil Science Society of America Journal* **44(5)**, 892-898.

Wardlaw N.C., Li, Y. and Forbes D., 1987. Pore-throat size correlation from capillary pressure curves. *Transport in Porous Media* **2(6)**, 597-614.

Wardlaw N.C., McKellar M. and Li Y., 1988. Pore and throat size distributions determined by mercury porosimetry and by direct observation. *Carbonates and Evaporites* **3(1)**, 1-16.

Wardlaw N.C. and Taylor R.P., 1976. Mercury capillary pressure curves and the interpretation of pore structure and capillary behaviour in reservoir rocks. *Bulletin of Canadian Petroleum Geology* **24(2)**, 225-262.

Watts N.L., 1987. Theoretical aspects of cap-rock and fault seals for single and two-phase CO_2 columns. *Marine and Petroleum Geology* **4(4)**, 274-307.

Zeynaly-Andabily E.M. and Rahman S.S., 1995. Measurement of the permeability of tight rocks. *Measurement Science and Technology* **6(10)**, 1519-1527.

Zhou F., Hussain F. and Cinar Y., 2013. Injecting pure N_2 and CO_2 to coal for enhanced coalbed methane: experimental observations and numerical simulation. *International Journal of Coal Geology* **116-117**, 53-62.

Zieglar D.L., 1992. CO_2 columns, buoyancy pressures, and seal efficiency: comparisons of oil and gas accumulations in California and the Rocky Mountain area. *The American Association of Petroleum Geologists Bulletin* **76(4)**, 501-508.